Received 8 May 2022; accepted 1 June 2022. Date of publication 9 June 2022; date of current version 22 July 2022.

Digital Object Identifier 10.1109/OJCOMS.2022.3181812

Data Combining Schemes for a Detector Array Receiver in Free-Space Optical Communications

MING-CHENG TSAI (Graduate Student Member, IEEE), MUHAMMAD SALMAN BASHIR (Senior Member, IEEE), AND MOHAMED-SLIM ALOUINI (Fellow, IEEE)

Computer, Electrical and Mathematical Science and Engineering (CEMSE) Division, King Abdullah University of Science and Technology, Thuwal 23955-6900, Saudi Arabia

CORRESPONDING AUTHOR: M. S. BASHIR (e-mail: muhammad.bashir@fulbrightmail.org)

This work was supported by the Office of Sponsored Research (OSR) at King Abdullah University of Science and Technology (KAUST).

ABSTRACT An array of detectors is widely used in deep space optical communications for both fine beam tracking and symbol detection. In this paper, we have analyzed and compared the performance of different combining schemes—such as *equal gain combiner* (EGC), *selection combiner* (SC) and the *maximal ratio combiner* (MRC)—that are used to fuse the outputs from the elements of such arrays. The three combining schemes are compared in terms of error rate performance and computational complexity. Additionally, for the limiting case of continuous arrays of circular configuration, the optimization of two important parameters—the spot size and the array size—is also discussed in order to achieve the best error rate performance.

INDEX TERMS Array of detectors, equal gain combiner, free-space optics, maximal ratio combiner, probability of error, selection combiner.

I. INTRODUCTION

FREE-SPACE optics is slated to become an enabler of high data-rates in the backhaul of next generation of wireless communication networks due to the availability of large chunks of unused spectrum in the optical domain of the electromagnetic spectrum [1]. However, due to the narrow beamwidth associated with the optical signal (the beamwidth angle is proportional to $\frac{\lambda}{D}$ where λ is the wavelength of light and D is diameter of transmit aperture), pointing and tracking requirements have become more stringent for the performance of a FSO communications link. Thus, the pointing and tracking subsystems form an important part of a FSO communications receiver. At the receiver, the received light is focused on a detection element—which is either a single-detector or an array of detectors—that lies in the focal plane of the aperture lens. Typically, a non-coherent energy detection (*intensity modulation/direct detection* or IM/DD) scheme is used in FSO receivers because of its reduced hardware complexity as opposed to coherent receivers.

A. MOTIVATION

An array of detectors can be used jointly for symbol detection and beam tracking. This makes it an attractive alternative to a single detector receiver that requires separate tracking and detection channels (please see Fig. 2). For instance, [2] discusses an arrangement whereby the energy in the PPM signal pulse is used to infer the angle-of-arrival of the received beam in satellite communications in a joint beam tracking and data detection arrangement with an array of detectors. Such an arrangement renders a separate beam tracking assembly/channel unnecessary. As shown in Fig. 2, communications with a single detector require a split of received beam energy into the tracking (fraction $1-\alpha$ goes into the tracking channel) and symbol detection channels, whereas no such split is required in the arrangement in Fig. 3 where the same array is used both for symbol detection and beam tracking.

In the context of joint beam tracking and symbol detection, the performance of detector arrays in terms of beam tracking (estimation of angle-of-arrival) for moving platforms is

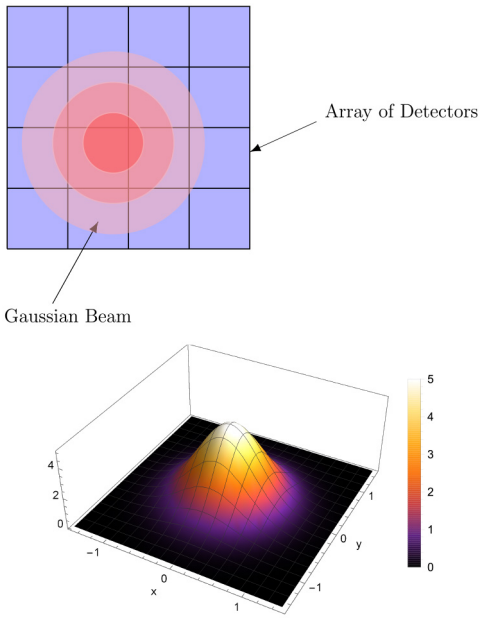

FIGURE 1. The figure on the top shows a 4 × 4 array of detectors receiver for FSO with the beam spot or airy pattern focused on the array. The figure on the bottom shows the intensity profile of the airy pattern modeled with a Gaussian function.

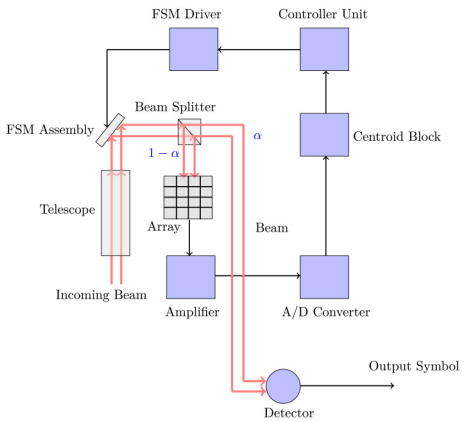

FIGURE 2. This figure shows the block diagram of a single-detector receiver. Only a fraction of received energy (denoted by α) goes into the data channel, and $(1-\alpha)$ finds its way into the tracking channel. The parameter α can be varied between 0 and 1 by turning a knob on a variable beam splitter.

discussed in detail in [2]. However, there is no study available in the literature that discusses and compares the symbol detection and error rate performance of an array of detectors in the context of data combining or fusion schemes. Therefore, in this study, we want to fill this gap by examining and comparing the system performance—in terms of error probability and computational complexity—of different combining schemes (such as equal gain combining, selection combining and maximal ratio combining) for an array of detectors. The use of these different schemes to combine the output of each element is validated by noting the fact that the distribution of energy on the array is nonuniform, and the intensity distribution is modeled by a two dimensional circularly symmetric Gaussian distribution [3] in most scenarios as shown in Fig. 1. Thus, if the distribution of intensity is nonuniform and the distribution obeys a certain

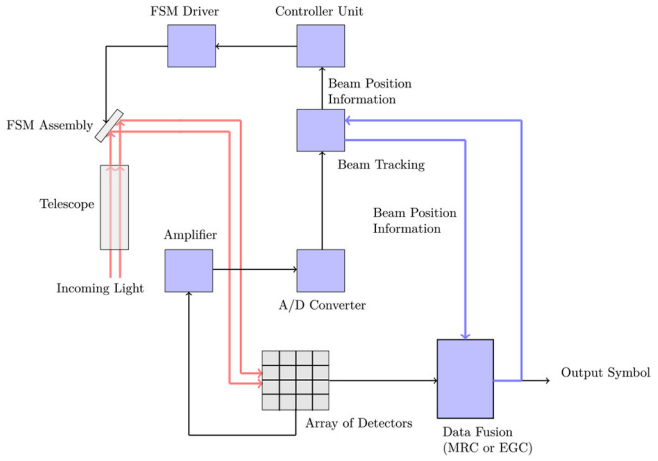

FIGURE 3. This figure shows the block diagram of a detector array receiver.

model (such as a Gaussian model in our case), then applying different combining or fusing algorithms can lead to a change—or perhaps an improvement—in the performance (such as error probability performance) of the system. Thus, we are motivated in the current study to apply different combining schemes to the outputs of array elements in order to maximize the error rate performance of the FSO receiver. Here, we want to emphasize that in contrast to the conventional combining schemes for the radio frequency systems that provide diversity against channel fading, the optimal and suboptimal combining of the outputs of the elements of the array in an FSO channel is useful even when no fading of the optical signal occurs. In this regard, the combining schemes exploit the variation in the beam intensity on the array in order to maximize this performance, and this variation in energy happens even when the signal does not undergo fading.

B. BACKGROUND LITERATURE REVIEW AND CONTRIBUTIONS OF THIS STUDY

There are a number of studies in the literature that deal with beam acquisition and beam tracking with detector arrays in a free-space optical communications receiver. For instance, regarding tracking, the authors in [4], [5] have proposed beam position estimation and tracking algorithms for a photon-counting detector array receiver concerning a joint beam position tracking and symbol detection scheme for PPM symbols in satellite communications. The authors in [6] analyze the probability of error in detail for the joint beam position tracking and symbol detection system, and show that the probability of error of a maximal ratio combining scheme is minimized if the beam is tracked accurately enough in time. The authors in [7] consider time synchronization schemes for a detector array receiver in a photon-counting channel in deep space optical communications. The authors in [8] have considered the performance of the communications for an array of detectors and discussed the effects of the number of detectors and the beam parameter information on the performance. They showed that for a maximal ratio combining scheme, the probability of error

decays monotonically with the number of detectors in the array if the area of the array is kept fixed. The authors in [9] have discussed the signal acquisition performance obtained with an array of detectors receiver for a photon-counting optical channel. In that work, they have quantified the effect of the number of detectors on the acquisition performance of the system. The work [10] analyzes the performance of a free-space optical multiple-input single-output receiver for noncoherent and coherent beam combining schemes and pointing errors. Additionally, the performance of an array of detectors receiver in a deep-space optical communications has been discussed in [11], [12], [13], and these three studies provide an excellent read on this topic. In the aforementioned papers, the authors have discussed the effect of the non-uniform weighting of array elements on the performance of centroid tracking and symbol detection performance of the receiver. Finally, the studies [14], [15], [16] discuss novel nonlinear strategies with an array of photodetectors that minimize the effect of background radiation in order to enhance the SNR at the receiver.

Regarding pointing errors, the authors in [17] consider the optimization of outage capacity of an FSO link in terms of the beam radius. The link employs a single detector at the receiver, and the outage capacity is optimized for a Gaussian beam. The authors in [18] examine the maximization of link availability as a function of beam radius for a single-detector FSO receiver.

Finally, references [19], [20], [21] present a good overview of diversity combining schemes in wireless communications.

In the current study, we want to extend the work carried out in [2] where we had considered the tracking performance of an array of detectors in terms of Cramér-Rao bounds for a joint communications and beam tracking system. In this paper, we have analyzed and compared the bit error rate performance that can be achieved with an array of detectors in the communications mode (without considering tracking into account). In this regard, we have examined and compared the performance of different data combining schemes such as the equal gain combiner (EGC), maximal ratio combiner (MRC), and the selection combiner (SC), which are used to combine the outputs of each element of the array. We have examined the performance of these combining schemes for different values of spot sizes and the number of elements in the array. As a limiting case, we have also considered the performance in the limit as the number of detectors goes to infinity for a fixed-size array (we call such a limiting array the "continuous" array as opposed to a "discrete" array which has a finite number of elements). The motivation for using the continuous array in our analysis has been discussed in Section III. Finally, we have considered optimizing the beam or spot size in the focal plane and the area of the array (which is placed in the focal plane) for the continuous array case.

C. MODEL ASSUMPTIONS

Without a loss of generality, we make the following assumptions before we begin the analysis in this study:

1) Strictly speaking, the intensity distribution on the focal plane is the Fourier Transform of the intensity distribution impinging on the telescope aperture. Assuming a circular aperture, the resulting intensity distribution of the airy pattern on the focal plane is represented by a scaled Bessel function in two dimensions [22]. Because of the mathematical tractability afforded by Gaussian functions, we have approximated the shape of the airy pattern by a circularly symmetric Gaussian distribution in two dimensions [3].
2) We assume that the received signal power is large enough so that enough photons are received for the Gaussian approximation of the Poisson process to hold. For large values of received signal photon rate, the shot noise variance will depend on the received signal power. However, we assume that the thermal noise dominates the signal dependent shot noise, and therefore, a signal independent zero-mean Gaussian noise distribution is assumed in this study.
3) We assume that the noise intensity is distributed uniformly over the array. The noise results due to the thermal effect that leads to dark current in detectors as well as the unwanted background radiation that finds its way through the optical filters onto the surface of the array. We model the sum of all noise sources by a zero-mean Gaussian distribution with noise power density N_0 which is measured in terms of Watts per unit area.
4) The shape of the array is a square, and the shape of each detector in the array is also assumed to be square. The square shape of each detector in the array helps the detectors fill up the entire space inside the array. Thus, the optical fill factor of a hundred percent is assumed in this case.[1] We use a circular array configuration during the optimization phase because a circular array is easier to analyze mathematically in the presence of a circularly symmetric Gaussian beam.
5) Regarding the received signal power, we consider a classical inference viewpoint instead of the Bayesian inference model in this paper. This implies that the received signal amplitude is assumed to be an unknown constant quantity instead of being modeled by a random process. The Bayesian model will be considered in a future study on this topic.
6) In this study, we have considered the effect of pointing error on the optimization of system parameters (discussed in Section IV-A.1). The pointing error results either due to the atmospheric turbulence or because of the mechanical vibrations in the transmitter and receiver assemblies. However, the scintillation of the beam due to atmospheric turbulence is not considered since the Gaussian approximation of spot energy on the focal plane may not hold under severe scintillation.

1. Even if the optical fill factor is less than a hundred percent, we can get close to a hundred percent effect by placing a microlens array before the array of detectors in the focal plane.

Notation	Name & Units
ρ	beam or spot radius (mm)
(x_0, y_0)	beam center location
λ_p	total power in the airy pattern or beam spot (Watts)
$\frac{\lambda_p}{2\pi\rho^2}$	peak signal intensity (Watts)
N_0	noise parameter (Watts/mm^2)
σ^2	total array noise power (Watts)
M	number of detectors in the array
$\lvert\mathcal{A}\rvert$	area of detector array (mm^2)
$\mathcal{M}$	PPM modulation order
Λ_m	projected signal intensity on mth detector of the array (Watts)
R	radius of circular array (mm)
$\mathbb{L}$	length of one side of square array (mm)
α	normalized length of one side of square array: $\alpha := \mathbb{L}/\rho$.
σ_p	pointing error standard deviation (mm)

FIGURE 4. List of Mathematical Symbols.

Therefore, we assume that either the adaptive optics assembly inside the receiver is able to make wavefront corrections effectively so as to minimize the scintillation effect, or that the turbulent eddies are large enough in size so as to only bend the beam's direction instead of "breaking" the beam into smaller components that leads to the scintillation effect.

D. ORGANIZATION OF THIS PAPER

This paper is organized as follows. Section II defines the system model in terms of a Gaussian beam and the array of detectors. In the same section, we lay out the error probability expressions concerning the different combining schemes that are used to combine the outputs of the elements of the array. Section III considers optimization of system parameters (spot and array areas) for a continuous circular array. Section IV discuss the simulation and experimental results in detail. Finally, Section V argues a brief complexity analysis of different combining schemes, and Section VI sums up the conclusions of our study and discusses future work in the direction of the current study.

Fig. 4 shows the list of important mathematical symbols used in this paper.

II. PROBABILITY OF ERROR OF AN ARRAY OF DETECTORS

The intensity distribution of the spot or airy pattern impinging on the focal plane array (detector array in the focal plane) is described by a Gaussian distribution:

$$\Lambda(x, y) = \frac{\lambda_p}{2\pi\rho^2} \exp\left(-\frac{(x-x_0)^2 + (y-y_0)^2}{2\rho^2}\right) \cdot \mathbb{1}_{\mathcal{A}}(x, y), \tag{1}$$

where $\frac{\lambda_p}{2\pi\rho^2}$ is known as the peak intensity of the spot, ρ is known as the effective spot or beam radius on the focal plane, and (x_0, y_0) represent the center of the beam on the focal plane. The factor λ_p is the total power in the spot or airy pattern in Watts. We assume that the center of the array lies at the origin $(0, 0)$. The factor $\mathbb{1}_A$ is the indicator function on some measurable set A and $\mathcal{A}$ represents the region of the detector array.

The total current of the array due to thermal and background noise is modeled by a zero-mean Gaussian random variable whose variance is given by the factor $N_0|\mathcal{A}|$ where N_0 is the noise power per unit area and $|\mathcal{A}|$ represents the area of the detector array. The output of the mth detector in the array is given by

$$Y_m = \Lambda_m + N_m \tag{2}$$

where Λ_m is the signal power in the mth detector of the array: $\Lambda_m \triangleq \iint_{A_m} \Lambda(x, y)\, dy\, dx$, where A_m is the region of the mth detector. The quantity N_m is a Gaussian random variable that represents noise in the mth detector and its distribution is defined as $N_m \sim \mathcal{N}(0, N_0 \frac{|\mathcal{A}|}{M})$. Here, M represents the total number of detectors in the array.

A. EQUAL GAIN COMBINER

It can be shown that—for the pulse position modulation (PPM) scheme—the probability of error obtained with an array of detectors for an equal gain combining scheme is given by [10]

$$\mathbb{P}(\mathcal{E}) = 1 - \left(Q\left(-\frac{\sum_{m=1}^{M} \Lambda_m}{\sqrt{2N_0\mathcal{A}}}\right)\right)^{\mathcal{M}-1}, \tag{3}$$

where $\mathcal{M}$ is the PPM order which is equal to the number 2^n for a positive integer n. The function $Q(\cdot)$ is the tail distribution function of a standard normal random variable.

B. MAXIMAL RATIO COMBINER

For the $\mathcal{M} - PPM$, it can be shown that the probability of error of the maximal ratio combiner is [10]

$$\mathbb{P}(\mathcal{E}) = 1 - \left(Q\left(-\sqrt{\frac{\sum_{m=1}^{M} \Lambda_m^2}{2N_0 \frac{|\mathcal{A}|}{M}}}\right)\right)^{\mathcal{M}-1}. \tag{4}$$

C. SELECTION COMBINER (MAX SNR)

In this case, we choose the detector with the highest signal power (or SNR since the noise power in each detector is the same). For this scenario, we note that the information concerning beam center location (x_0, y_0) is required in order to select the detector with the maximum SNR. For SC (Max SNR), we choose a detector of the array whose signal power is

$$\Lambda_{\max} \triangleq \max(\Lambda_1, \Lambda_2, \ldots, \Lambda_M). \tag{5}$$

Here we want to address one important point. The quantity Λ_m is the signal power in the mth detector, and since the noise power in each detector is known, the SNR of any detector can be computed easily by figuring out the signal power in the detector. In order to compute the signal power in a particular detector, we need to know the spot size or radius ρ and the location of the spot on the array (x_0, y_0). If we have a knowledge (or estimate) of these two quantities,

we can easily compare the SNR of each detector with any other detector of the array. In this sense, the detector with the maximum SNR can be located based on $\hat{\rho}$ and $(\hat{x}_0, \hat{y}_0)$ where $\hat{\rho}$ is the estimate of ρ and $(\hat{x}_0, \hat{y}_0)$ is the estimate of (x_0, y_0).[2] If the estimates are poorer, we may falsely declare that a certain detector contains the maximum SNR which may not actually be the case. Therefore, accurate estimation of ρ and (x_0, y_0) is quite important for the computation of a sufficient statistic based on SC (Max SNR) combining scheme.

The output of the detector containing the maximum SNR is denoted by Y_s during a PPM signal slot, and Y_n denotes the output of the same detector during a noise-only slot. For $\mathcal{M}$-PPM, the probability of a correct decision in this case is

$$\mathbb{P}(\mathcal{C}) = (\mathbb{P}(\{Y_s > Y_n\}))^{\mathcal{M}-1}. \tag{6}$$

We know that $Y_s \sim \mathcal{N}(\Lambda_{\mathsf{max}}, N_0\frac{|\mathcal{A}|}{M})$ $Y_n \sim \mathcal{N}(0, N_0\frac{|\mathcal{A}|}{M})$. Then $P(\mathcal{C}) = (F_{Y_n}(Y_s))^{\mathcal{M}-1}$ which implies that the conditional probability is

$$\mathbb{P}(\{Y_n < Y_s\}|\{Y_s = y\}) = F_{Y_n}(y) = Q\left(-\frac{y}{\sqrt{N_0\frac{|\mathcal{A}|}{M}}}\right). \tag{7}$$

Therefore,

$$\mathbb{P}(\{Y_n < Y_s\}) = \int_{-\infty}^{\infty} Q\left(-\frac{y}{\sqrt{N_0\frac{|\mathcal{A}|}{M}}}\right) f_{Y_s}(y)\, dy \tag{8}$$

where

$$f_{Y_s}(y) = \frac{1}{\sqrt{2\pi N_0\frac{|\mathcal{A}|}{M}}} \exp\left(-\frac{(y-\Lambda_{\mathsf{max}})^2}{2N_0\frac{|\mathcal{A}|}{M}}\right). \tag{9}$$

Thus,

$$\begin{aligned}\mathbb{P}(\mathcal{E}) &= 1 - \mathbb{P}(\mathcal{C}) \\ &= 1 - \left(\int_{-\infty}^{\infty} Q\left(-\frac{y}{\sqrt{N_0\frac{|\mathcal{A}|}{M}}}\right) f_{Y_s}(y)\, dy\right)^{\mathcal{M}-1}.\end{aligned} \tag{10}$$

1) ASYMPTOTIC RESULT: $M \to \infty$

For large M, the signal energy in the detector having maximum SNR is approximately

$$S \approx \frac{\lambda_p}{2\pi\rho^2}\frac{|\mathcal{A}|}{M}. \tag{11}$$

Thus, in this case, the probability of error expression concerning an $\mathcal{M}$-PPM scheme for large M is

$$\begin{aligned}\mathbb{P}(\mathcal{E}) &\approx 1 - \left(Q\left(-\frac{\frac{\lambda_p}{2\pi\rho^2}\frac{|\mathcal{A}|}{M}}{\sqrt{2N_0\frac{|\mathcal{A}|}{M}}}\right)\right)^{\mathcal{M}-1} \\ &= 1 - \left(Q\left(-\frac{\frac{\lambda_p}{2\pi\rho^2}\sqrt{\frac{|\mathcal{A}|}{M}}}{\sqrt{2N_0}}\right)\right)^{\mathcal{M}-1}.\end{aligned} \tag{12}$$

Since $M \to \infty \implies \frac{|\mathcal{A}|}{M} \to 0$, for (12) we have that

$$\lim_{M\to\infty} \mathbb{P}(\mathcal{E}) = 1 - \left(\frac{1}{2}\right)^{\mathcal{M}-1}, \tag{13}$$

and we note that the error probability is 0.5 when $\mathcal{M} = 2$.

2) SIMPLER EXPRESSION FOR HIGH SNR CASE

When the SNR is high, that is, $\Lambda_{\mathsf{max}} >> N_0\frac{|\mathcal{A}|}{M}$, then (9) can be approximated by a Dirac delta function: $f_{Y_s}(y) \approx \delta(y - \Lambda_{\mathsf{max}})$. Thus, for this asymptotic case of high SNR, expression (10) becomes

$$\begin{aligned}\mathbb{P}(\mathcal{E}) &= 1 - \left(\int_{-\infty}^{\infty} Q\left(-\frac{y}{\sqrt{N_0\frac{|\mathcal{A}|}{M}}}\right) f_{Y_s}(y)\, dy\right)^{\mathcal{M}-1} \\ &= 1 - \left(\int_{-\infty}^{\infty} Q\left(-\frac{y}{\sqrt{N_0\frac{|\mathcal{A}|}{M}}}\right) \delta(y-\Lambda_{\mathsf{max}})\, dy\right)^{\mathcal{M}-1} \\ &= 1 - \left(Q\left(-\frac{\Lambda_{\mathsf{max}}}{\sqrt{N_0\frac{|\mathcal{A}|}{M}}}\right)\right)^{\mathcal{M}-1}.\end{aligned} \tag{14}$$

D. SELECTION COMBINER (MAX OUTPUT)

In the selection combining (Max Output) scheme—as the name depicts—we choose the detector with the largest output to detect the symbol. For the signal slot of a PPM symbol:

$$Y^{(s)}_{\mathsf{max}} \triangleq \max\left(Y^{(s)}_1, Y^{(s)}_2, \ldots, Y^{(s)}_M\right), \tag{15}$$

where $Y^{(s)}_m \sim \mathcal{N}(\Lambda_m, N_0\frac{|\mathcal{A}|}{M})$. Similar to this argument, we have that for a noise-only slot,

$$Y^{(n)}_{\mathsf{max}} \triangleq \max\left(Y^{(n)}_1, Y^{(n)}_2, \ldots, Y^{(n)}_M\right), \tag{16}$$

where $Y^{(n)}_m \sim \mathcal{N}(0, N_0\frac{|\mathcal{A}|}{M})$. Now,

$$\mathbb{P}(\mathcal{C}) = \left(\mathbb{P}\left(\left\{Y^{(s)}_{\mathsf{max}} > Y^{(n)}_{\mathsf{max}}\right\}\right)\right)^{\mathcal{M}-1}. \tag{17}$$

In this case,

$$\begin{aligned}&\mathbb{P}\left(\left\{Y^{(n)}_{\mathsf{max}} < Y^{(s)}_{\mathsf{max}}\right\}\middle|\left\{Y^{(s)}_{\mathsf{max}} = y\right\}\right) \\ &= \mathbb{P}\left(\left\{Y^{(n)}_{\mathsf{max}} < y\right\}\right) \\ &= \mathbb{P}\left(\left\{Y^{(n)}_1 < y\right\} \cap \left\{Y^{(n)}_2 < y\right\} \cap \ldots \cap \left\{Y^{(n)}_M < y\right\}\right) \\ &= \left(Q\left(-\frac{y}{\sqrt{N_0\frac{|\mathcal{A}|}{M}}}\right)\right)^{M}.\end{aligned} \tag{18}$$

The cumulative distribution function of $Y^{(s)}_{\mathsf{max}}$ is

$$F_{Y_{\mathsf{max}}}(y) \triangleq \mathbb{P}\left(\left\{Y^{(s)}_{\mathsf{max}} < y\right\}\right)$$

2. In case the turbulence-induced scintillation is negligible, we can infer ρ easily based on the focal length of the aperture lens.

$$= \mathbb{P}\left(\left\{Y_1^{(s)} < y\right\} \cap \left\{Y_2^{(s)} < y\right\} \cap \ldots \cap \left\{Y_M^{(s)} < y\right\}\right) \tag{19}$$

$$= \prod_{m=1}^{M} Q\left(-\frac{(y-\Lambda_m)}{\sqrt{N_0 \frac{|\mathcal{A}|}{M}}}\right). \tag{20}$$

Since $\frac{\partial}{\partial x}Q(x) = -\frac{1}{\sqrt{2\pi}}\exp(-\frac{x^2}{2})$, we have that the probability density function of $Y_{\mathsf{max}}^{(s)}$ is

$$f_{Y_{\mathsf{max}}}(y) = \sum_{m=1}^{M}\left(\frac{\partial}{\partial y}Q\left(-\frac{(y-\Lambda_m)}{\sqrt{N_0\frac{|\mathcal{A}|}{M}}}\right)\prod_{\substack{i=1\\ i\neq m}}^{M} Q\left(-\frac{(y-\Lambda_i)}{\sqrt{N_0\frac{|\mathcal{A}|}{M}}}\right)\right)$$
$$= \sum_{m=1}^{M}\left(\frac{1}{\sqrt{2\pi N_0\frac{|\mathcal{A}|}{M}}}\exp\left(-\frac{(y-\Lambda_m)^2}{2N_0\frac{|\mathcal{A}|}{M}}\right)\prod_{\substack{i=1\\ i\neq m}}^{M} Q\left(-\frac{(y-\Lambda_i)}{\sqrt{N_0\frac{|\mathcal{A}|}{M}}}\right)\right). \tag{21}$$

Therefore,

$$\mathbb{P}\left(\left\{Y_{\mathsf{max}}^{(n)} < Y_{\mathsf{max}}^{(s)}\right\}\right) = \int_{-\infty}^{\infty}\left(Q\left(-\frac{y}{\sqrt{N_0\frac{|\mathcal{A}|}{M}}}\right)\right)^M f_{Y_{\mathsf{max}}}(y)\,dy, \tag{22}$$

where $f_{Y_{\mathsf{max}}}(y)$ is given by (21). Finally, the error probability is

$$\mathbb{P}(\mathcal{E}) = 1 - \mathbb{P}(\mathcal{C}) = 1 - \left(\int_{-\infty}^{\infty}\left(Q\left(-\frac{y}{\sqrt{N_0\frac{|\mathcal{A}|}{M}}}\right)\right)^M f_{Y_{\mathsf{max}}}(y)\,dy\right)^{\mathcal{M}-1}. \tag{23}$$

1) ASYMPTOTIC RESULT: $M \to \infty$

For the noise-only slot of $\mathcal{M}$-PPM, we know (from (18)) that the maximum output—denoted by $Y_{\mathsf{max}}^{(n)}$—has the cumulative distribution given by $F(y) = (Q(-\frac{y}{\sqrt{N_0\frac{|\mathcal{A}|}{M}}}))^M$. For the case of the slot containing the signal pulse, the cumulative distribution function of the maximum output—denoted by $Y_{\mathsf{max}}^{(s)}$—is

$$F(y) = \prod_{m=1}^{M} Q\left(-\frac{(y-\Lambda_m)}{\sqrt{N_0\frac{|\mathcal{A}|}{M}}}\right). \tag{24}$$

For large M, $\Lambda_m \approx \mathcal{S}_m\frac{|\mathcal{A}|}{M}$ where $\mathcal{S}_m = \frac{\lambda_p}{2\pi\rho^2}\exp(-\frac{(x_m-x_0)^2+(y_m-y_0)^2}{2\rho^2})$, where (x_m, y_m) denotes the center of the mth detector. Therefore, for large M,

$$F(y) \approx \prod_{m=1}^{M} Q\left(-\frac{\left(y-\mathcal{S}_m\frac{|\mathcal{A}|}{M}\right)}{\sqrt{N_0\frac{|\mathcal{A}|}{M}}}\right) = \prod_{m=1}^{M} Q\left(-\frac{y}{\sqrt{N_0\frac{|\mathcal{A}|}{M}}} + \frac{\mathcal{S}_m\sqrt{\frac{|\mathcal{A}|}{M}}}{\sqrt{N_0}}\right) \tag{25}$$

and since $\frac{|\mathcal{A}|}{M} \approx 0$ for large M,

$$F(y) \approx \prod_{m=1}^{M} Q\left(-\frac{y}{\sqrt{N_0\frac{|\mathcal{A}|}{M}}}\right) = \left(Q\left(-\frac{y}{\sqrt{N_0\frac{|\mathcal{A}|}{M}}}\right)\right)^M. \tag{26}$$

Comparing (24) and (26), we note that $Y_{\mathsf{max}}^{(s)}$ and $Y_{\mathsf{max}}^{(n)}$ are identically distributed and independent for large M. In this case, $P(\{Y_{\mathsf{max}}^{(s)} > Y_{\mathsf{max}}^{(n)}\}) = \frac{1}{2}$ which can be shown by the following argument. For two identically distributed random variables X and Y, $F_X(z) = F_Y(z) = F(z)$, where $F_X(\cdot)$ and $F_Y(\cdot)$ are cumulative distribution functions of X and Y, respectively. Then, the probability that $Y < X$ is,

$$\mathbb{P}(\{Y < X\}) = \int_{-\infty}^{\infty}\mathbb{P}(\{Y < x\})\,dF(x) = \int_{-\infty}^{\infty}F(x)\,dF(x) = \int_0^1 u\,du = \frac{1}{2}. \tag{27}$$

Therefore, for large M, the probability of error for SC (Max Output) is

$$\lim_{M\to\infty}\mathbb{P}(\mathcal{E}) = 1 - \left(\frac{1}{2}\right)^{\mathcal{M}-1}, \tag{28}$$

which is the same as the asymptotic error probability for SC (Max SNR).

III. OPTIMIZATION OF DETECTOR ARRAY PARAMETERS FOR CONTINUOUS ARRAY APPROXIMATION

For optimization, we consider a continuous approximation of a practical or discrete detector array (a discrete array is an array made up of a finite number of elements). The continuous approximation implies the limiting case where the number of elements M goes to infinity for the fixed array area $|\mathcal{A}|$. This implies that the area of each detector in the array is shrinking to zero, and we are dealing with a large number of "point" detectors. The continuous approximation is required in order to solve the optimization problems that follow in this section. The continuous array approximation is justified as discussed in [23] where it was shown that the continuous array performance is substantially close to the performance of a finite M array if the dimensions of each detector are much smaller than the footprint $2\pi\rho^2$ of the spot. For instance, the tracking performance of 6×6 (36 detectors in the array) or higher resolution arrays is close to the continuous array's performance if the beam footprint $2\pi\rho^2$ is approximately the same size as the array.

Since the performance of EGC does not depend on M, the EGC's performance is the same whether a discrete array is used or its continuous analog. However, as we will note later,

the performance of MRC improves when M is large. Hence, for the MRC scheme, the error probability for the continuous array acts as a lower bound on the error probability for any array with a finite number of detectors.

Now we consider the continuous approximation of the array by taking M to infinity while holding the area $|\mathcal{A}|$ of the array constant. The output of the mth detector of the array is

$$Y_m = \Lambda_m + N_m \tag{29}$$

where $\Lambda_m = \iint_{A_m} \frac{\lambda_p}{2\pi\rho^2} e^{-\frac{(x-x_0)^2+(y-y_0)^2}{2\rho^2}}\, dx\, dy$. For large M,

$$Y_m = \frac{\lambda_p}{2\pi\rho^2} e^{-\frac{(x_m-x_0)^2+(y_m-y_0)^2}{2\rho^2}} \Delta_M + N_m \tag{30}$$

where $N_m \sim \mathcal{N}(0, N_0\Delta_M)$, N_0 is noise power per unit area, and $\Delta_M \triangleq \frac{A}{M}$ is the area of each (small) cell. The output of the MRC is

$$\begin{aligned} Z &= \sum_{m=1}^{M} \left(\frac{\lambda_p}{2\pi\rho^2} e^{-\frac{(x_m-x_0)^2+(y_m-y_0)^2}{2\rho^2}} \Delta_M e^{-\frac{(x_m-x_0)^2+(y_m-y_0)^2}{2\rho^2}} \right. \\ &\qquad \left. + N_m e^{-\frac{(x_m-x_0)^2+(y_m-y_0)^2}{2\rho^2}} \right) \\ &= \underbrace{\sum_{m=1}^{M} \frac{\lambda_p}{2\pi\rho^2} e^{-\frac{(x_m-x_0)^2+(y_m-y_0)^2}{2\rho^2}} \Delta_M e^{-\frac{(x_m-x_0)^2+(y_m-y_0)^2}{2\rho^2}}}_{S} \\ &\quad + \underbrace{\sum_{m=1}^{M} N_m e^{-\frac{(x_m-x_0)^2+(y_m-y_0)^2}{2\rho^2}}}_{N} \end{aligned} \tag{31}$$

where $N \sim \mathcal{N}(0, N_0\Delta_M \sum_{m=1}^{M} e^{-(\frac{(x_m-x_0)^2+(y_m-y_0)^2}{\rho^2})})$. As $M \to \infty$,

$$S \to \iint_{\mathcal{A}} \frac{\lambda_p}{2\pi\rho^2} e^{-\frac{(x-x_0)^2+(y-y_0)^2}{\rho^2}}\, dx\, dy \tag{32}$$

and the variance of N approaches

$$\mathsf{Var}[N] \to N_0 \iint_{\mathcal{A}} e^{-\frac{(x-x_0)^2+(y-y_0)^2}{\rho^2}}\, dx\, dy. \tag{33}$$

For EGC, the sufficient statistic is given by

$$\begin{aligned} Z &= \sum_{m=0}^{M-1} Y_m \\ &= \sum_{m=0}^{M-1} \frac{\lambda_p}{2\pi\rho^2} e^{-\frac{(x_m-x_0)^2+(y_m-y_0)^2}{2\rho^2}} \Delta_M + N \end{aligned} \tag{34}$$

where $N := \sum_{m=0}^{M-1} N_m$. The quantity N is a zero-mean Gaussian random variable with variance $N_0|\mathcal{A}|$. It can be shown that as $M \to \infty$,

$$\mathbb{E}[Z] \to \iint_{\mathcal{A}} \frac{\lambda_p}{2\pi\rho^2} e^{-\frac{(x-x_0)^2+(y-y_0)^2}{2\rho^2}}\, dy\, dx \tag{35}$$

and $\mathsf{Var}[Z] = N_0|\mathcal{A}|$.

A. ERROR PROBABILITY AND CHANNEL CAPACITY EXPRESSIONS FOR CONTINUOUS ARRAY

For the on-off keying (OOK) scheme, the error probability for MRC is

$$\begin{aligned} P(\mathcal{E}) &= Q\left(\frac{\frac{\lambda_p}{2\pi\rho^2} \iint_{\mathcal{A}} e^{-\frac{(x-x_0)^2+(y-y_0)^2}{\rho^2}}\, dx\, dy}{2\sqrt{N_0}\sqrt{\iint_{\mathcal{A}} e^{-\frac{(x-x_0)^2+(y-y_0)^2}{\rho^2}}\, dx\, dy}} \right) \\ &= Q\left(\frac{\frac{\lambda_p}{2\pi\rho^2}\sqrt{\iint_{\mathcal{A}} e^{-\frac{(x-x_0)^2+(y-y_0)^2}{\rho^2}}\, dx\, dy}}{2\sqrt{N_0}} \right). \end{aligned} \tag{36}$$

The expression (36) is a general expression that applies to any array configuration. It can be easily shown that for the EGC,

$$P(\mathcal{E}) = Q\left(\frac{\frac{\lambda_p}{2\pi\rho^2} \iint_{\mathcal{A}} e^{-\frac{(x-x_0)^2+(y-y_0)^2}{2\rho^2}}\, dx\, dy}{2\sqrt{N_0}\sqrt{|\mathcal{A}|}} \right). \tag{37}$$

For the selection combining scheme, we note that

$$P(\mathcal{E}) \geq \lim_{M\to\infty} Q\left(\frac{\left(\frac{\lambda_p}{2\pi\rho^2}\frac{|\mathcal{A}|}{M}\right)}{2\sqrt{N_0}\sqrt{\frac{|\mathcal{A}|}{M}}} \right) = \frac{1}{2}. \tag{38}$$

The channel capacity for the maximal ratio combining scheme is given by

$$\begin{aligned} \mathcal{C} &= \ln\left(1 + \frac{\left(\iint_{\mathcal{A}} \frac{\lambda_p}{2\pi\rho^2} e^{-\frac{(x-x_0)^2+(y-y_0)^2}{\rho^2}}\, dy\, dx \right)^2}{N_0 \iint_{\mathcal{A}} e^{-\frac{(x-x_0)^2+(y-y_0)^2}{\rho^2}}\, dy\, dx} \right) \\ &= \ln\left(1 + \left(\frac{\lambda_p}{2\pi\sqrt{N_0}\rho^2} \right)^2 \iint_{\mathcal{A}} e^{-\frac{(x-x_0)^2+(y-y_0)^2}{\rho^2}}\, dy\, dx \right). \end{aligned} \tag{39}$$

Moreover, the channel capacity of the equal gain combining scheme is given by

$$\mathcal{C} = \ln\left(1 + \frac{\left(\iint_{\mathcal{A}} \frac{\lambda_p}{2\pi\rho^2} e^{-\frac{(x-x_0)^2+(y-y_0)^2}{2\rho^2}}\, dy\, dx \right)^2}{N_0|\mathcal{A}|} \right). \tag{40}$$

Finally, it follows from (38) that the channel capacity for the selection combining scheme for a continuous array is 0 nats/sec/Hz.

B. OPTIMIZATION OF BEAM RADIUS AND ARRAY AREA FOR A CIRCULAR DETECTOR ARRAY RECEIVER

Here, we optimize two system parameters, namely the spot radius and the array area, to optimize a particular objective

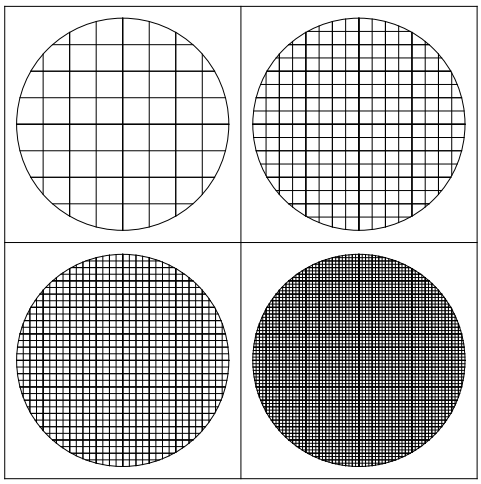

FIGURE 5. This figure shows a circular detector array with different number of detectors.

function (minimization of error probability or channel capacity). Without any loss of generality, we assume a circular array configuration since a circular array yields mathematically tractable analytical expressions that are easier to solve. In the first case, we assume no pointing error, i.e., the beam center and the array center are aligned which implies $x_0 = 0$ and $y_0 = 0$. In the second case, we consider optimization under pointing errors.

Fig. 5 shows circular detector arrays of the same area but with different numbers of detectors. The number of detectors increases from left to right and top to bottom. The bottom right figure shows the limiting case of the continuous array (the number of detectors is approaching infinity). The radius of all arrays is fixed at the number R.

1) MAXIMAL RATIO COMBINER

For a circular array configuration, we can use polar coordinates to write

$$\begin{aligned}&\iint_{\mathcal{A}} e^{-\frac{x^2+y^2}{\rho^2}}\,dx\,dy\\&=\int_{\theta=-\pi}^{\pi}\int_{r=0}^{R} r\exp\left(-\frac{r^2}{\rho^2}\right)dr\,d\theta\\&=\rho^2\pi\left(1-\exp\left(-\frac{R^2}{\rho^2}\right)\right),\end{aligned}\tag{41}$$

where R is the radius of the circular detector array. Thus, the probability of error for the MRC scheme of a circular array becomes

$$P(\mathcal{E}) = Q\left(\frac{\lambda_p\sqrt{\pi\rho^2\left(1-\exp\left(-\frac{R^2}{\rho^2}\right)\right)}}{4\pi\rho^2\sqrt{N_0}}\right).\tag{42}$$

We now need to solve the following optimization problem:

$$\begin{aligned}\underset{\rho,R}{\text{maximize}}\quad&\frac{\lambda_p\sqrt{2\pi\rho^2\left(1-\exp\left(-\frac{R^2}{2\rho^2}\right)\right)}}{4\pi\rho^2\sqrt{N_0}}\\\text{subject to}\quad&i)\ \rho_0<\rho<\rho_1,\\&ii)\ R_0<R<R_1.\end{aligned}\tag{43}$$

We note from (42) that in order to maximize the objective function, we need to i) minimize ρ and ii) maximize the array radius R. Thus, $\rho^* = \rho_0$ and $R^* = R_1$. We note that if $R_1 \gg 4\rho$, then choosing an $R > 4\rho$ will not lead to any significant gain in terms of error probability performance since most of the energy in the Gaussian beam is captured with an array of radius $R = 4\rho$.

2) EQUAL GAIN COMBINER

For the equal gain combiner, we need to solve the following optimization problem in order to minimize the error probability:

$$\begin{aligned}\underset{\rho,R}{\text{maximize}}\quad&\frac{\lambda_p 2\pi\rho^2\left(1-\exp\left(-\frac{R^2}{2\rho^2}\right)\right)}{4\pi^{\frac{3}{2}}\rho^2\sqrt{N_0}R}\\\text{subject to}\quad&i)\ \rho_0<\rho<\rho_1,\\&ii)\ R_0<R<R_1.\end{aligned}\tag{44}$$

In the optimization problem (44), we note that ρ should be as small as possible in order to maximize the objective function. Regarding the array radius R, we take the partial derivative of the objective function to R, and set the derivative equal to zero to obtain

$$R^2 - \rho_0^2\exp\left(\frac{R^2}{2\rho_0^2}\right) + \rho_0^2 = 0\tag{45}$$

The solution to this equation is obtained by setting $x = \frac{R^2}{2\rho_0^2}$ and rewriting (45) in terms of x as

$$2x + 1 = e^x.\tag{46}$$

Now, we manipulate (46) through several steps to finally obtain

$$\begin{aligned}2x+1 &= e^x\\&\implies -\left(x+\frac{1}{2}\right)\exp\left(-\left(x+\frac{1}{2}\right)\right)\\&= -\frac{1}{2\sqrt{\exp(1)}}\\&\implies W_{-1}\left(-\left(x+\frac{1}{2}\right)\exp\left(-\left(x+\frac{1}{2}\right)\right)\right)\\&= W_{-1}\left(-\frac{1}{2\sqrt{\exp(1)}}\right),\end{aligned}\tag{47}$$

where W_{-1} is the *Lambert W* function. Since $W_{-1}(z\exp(z)) = z$ for $z < 0$, we have that (47) is rewritten as

$$-\left(x+\frac{1}{2}\right) = W_{-1}\left(-\frac{1}{2\sqrt{\exp(1)}}\right).\tag{48}$$

Notation(s)	Name / Unit	Default Values
λ_p	peak power factor (Watt)	1
N_0	noise power (Watts/mm^2)	0.01
$\lvert\mathcal{A}\rvert$	area of array detector (mm^2)	4
ρ	beam radius (mm)	0.2
(x_0, y_0)	beam location (mm)	$(0, 0)$
M	number of Detectors	$16, 36, 64$
$\mathcal{M}$	PPM modulation order	8
σ_p	pointing error standard deviation (mm)	0, 0.05, 0.07

FIGURE 6. This table shows the default values for different system parameters concerning the experiments in this paper.

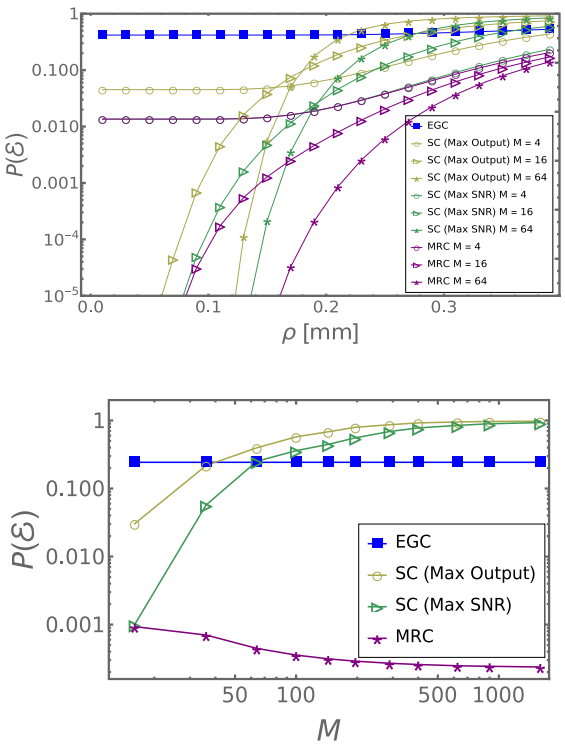

FIGURE 7. The figure on the top shows the error probability of different combining schemes as a beam radius ρ function. In contrast, the figure on the bottom shows the error probability as a function of the number of detectors M in the array.

By substituting the value of $x = \frac{R^2}{2\rho_0^2}$ into (48), we obtain the solution of optimum value of R:

$$R^* = \sqrt{-\rho_0^2\left(2W_{-1}\left(\frac{-1}{2\sqrt{\exp(1)}}\right)+1\right)}. \tag{49}$$

Thus, from (49), the optimum value of R is equal to constant times ρ_0 where the value of this constant is approximately 1.584762.

IV. SIMULATION RESULTS AND COMMENTARY

In this section, we summarise the simulation results on the performance comparison of the data combining schemes discussed in Sections II and III. The set of default parameter values is listed in Fig. 6.

Fig. 7 shows the error probability for different combining schemes as a function of spot radius ρ (left) and as a function

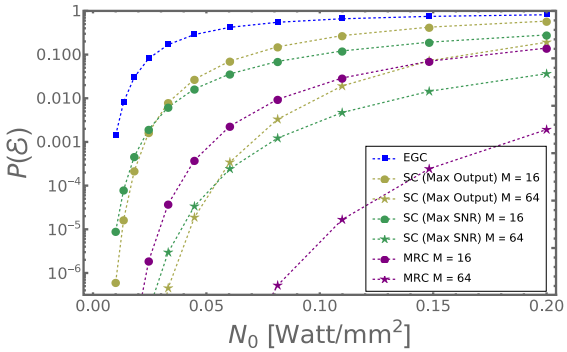

FIGURE 8. This figure shows the error probability of different combining schemes as a function of noise power N_0.

of a number of detectors M in the array (right). In this figure, we assume that the beam footprint is smaller than the area of the array, i.e., $2\pi\rho^2 < |\mathcal{A}|$. This assumption is essential if the array is to be used effectively for tracking the beam center on the array since the beam center's location on the array indicates the beam's angle of arrival. If the beam center and the array center are aligned, then the angle-of-arrival is zero; otherwise, the telescope direction and the fast steering mirror assembly must be adjusted to align the beam center with the array center to drive the angle-of-arrival to zero.

The performance of the EGC does not depend on ρ in the regime $2\pi\rho^2 < |\mathcal{A}|$ since EGC adds the (signal plus noise) output of each detector, and varying the beam radius will not affect the collected signal power by the array. Therefore, the error probability of the EGC is constant over the range of values ρ takes in Fig. 7. However, the performance of SC and MRC depend heavily on ρ since these schemes weight the output of each detector element nonuniformly. For the selection combiner of both types, we note that as the spot radius ρ increases relative to the size of each detector in the array, the performance of both the selection combining schemes begins to degrade. This is rather easily explained by the SNR of the output in the SC (Max SNR) case. For the square array, let us define $\mathbb{L}$ as the length of one side of the square array: $\mathbb{L} := \sqrt{|\mathcal{A}|}$. Then, the SNR (for M large and $\rho >> \mathbb{L}/M$) is given by equation (11) as

$$\text{SNR} = \frac{\left(\frac{\lambda_p}{2\pi\rho^2}\right)^2 \frac{|\mathcal{A}|}{M}}{2N_0}, \tag{50}$$

where we note that the SNR of the selection combiner will degrade as we increase M in the $\rho \gg \mathbb{L}/M$ regime.

Fig. 8 indicates the error rate performance of different combining schemes as a function of noise power N_0. We note that the performance of the two types of selection combiners converges for large SNR. This observation can be predicted from the fact that as the SNR improves, the detector with the most considerable output will converge to the detector with the largest SNR with high probability.

Figure 9 illustrates the effect of the estimation error—of two system parameters, namely the spot radius ρ and the spot

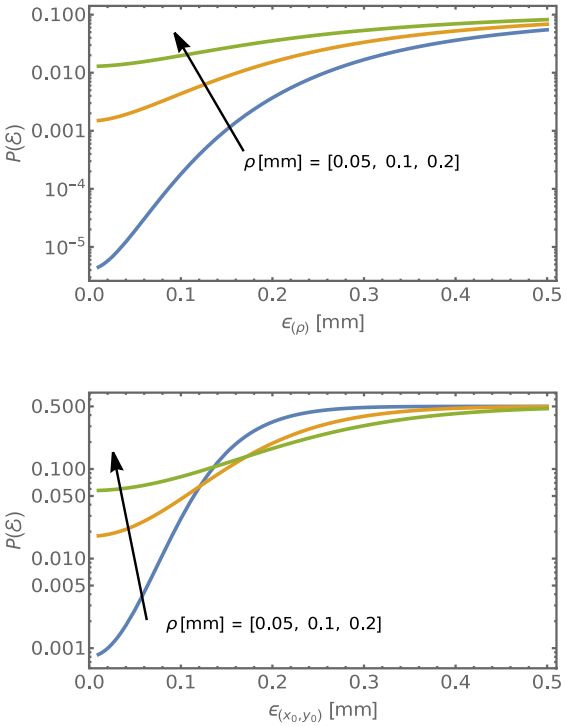

FIGURE 9. This figure shows the effect of estimation error on the maximal ratio combiner's performance. The figure on top depicts the effect of error in estimation of ρ and the bottom figure illustrates the performance degradation with estimation error for (x_0, y_0).

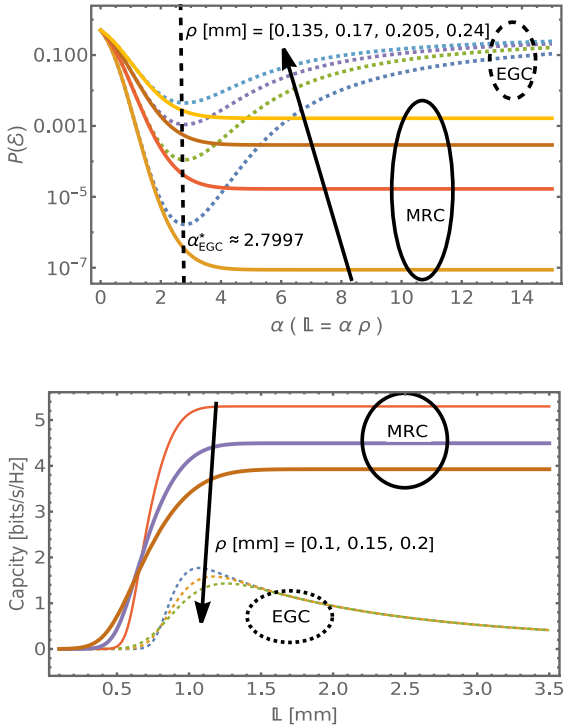

FIGURE 10. This figure shows the error probability (of the top) and the channel capacity (on the bottom) for the MRC and EGC schemes as a function of array parameters α and $\mathbb{L}$.

location (x_0, y_0)— on the performance of the MRC. For these plots, the signal power is 1 W, noise power is 0.05 W/mm^2, and the beam center (x_0, y_0) is fixed at the point the origin $(0, 0)$. The error $\epsilon(x_0, y_0) \coloneqq \sqrt{(\hat{x}_0 - x_0)^2 + (\hat{y}_0 - y_0)^2}$ and the error $\epsilon(\rho) \coloneqq \hat{\rho} - \rho$. We note that the performance of the MRC suffers as the errors $\epsilon(x_0, y_0)$, $\epsilon(\rho)$ grow.

A. RESULTS ON OPTIMIZATION OF BEAM PARAMETERS

Fig. 10 depicts the error probability as a function of the dimensions of a square array. The figure on the left side indicates error probability as a function of factor α where α is the normalized length of one of the four sides of a square-shaped array: $\alpha \coloneqq \frac{\mathbb{L}}{\rho}$. We observe that concerning the MRC, the length α should be as large as possible in order to minimize the error probability. This observation is corroborated by the optimization result obtained with a circular array where we had observed that the array dimensions have to be as large as possible in order to minimize the error probability. From this figure, we note that the effect of any increase in $\mathbb{L}$ beyond $\mathbb{L} = 4\rho$ is negligible because most of the energy in the Gaussian beam is captured within 4 standard deviations about the mean position.

Regarding the EGC, we note from the top subfigure of Fig. 10 that there is a certain α (or $\mathbb{L}$ or $|\mathcal{A}|$) that minimizes the error probability, and this α is constant for any ρ. This indicates that the optimal length $\mathbb{L}$ of the square array is a linear function of beam radius ρ, and the factor α is approximately 2.8 for the parameter values of our experiments. This observation is similar to the result for an optimum radius of the circular array obtained in Section III-B.2 where the optimum radius of the array was a constant multiple of the beam radius ρ. This implies that the optimum array area is proportional to the square of the beam radius for both the circular and square arrays.

The bottom subfigure in Fig. 10 depicts the channel capacity results related to the EGC and MRC arrays for a continuous array configuration.

Fig. 11 is a 3-D rendering of Fig. 10 (top) to show the dependence of the error probability on both the array length and the beam radius on the performance of the equal gain combiner.

1) OPTIMIZATION UNDER POINTING ERROR

In this section, we consider optimization of the beam parameter ρ when the beam or spot deviates from its mean position in the focal plane due to pointing error. The pointing error is induced either because of atmospheric turbulence, or due to mechanical vibrations in the transmitter and receiver assemblies. We consider the case when the pointing error is modeled by a Rayleigh random variable, i.e., the error is a zero-mean Gaussian random variable in each of the x and y dimensions with a uniform variance σ_p^2.

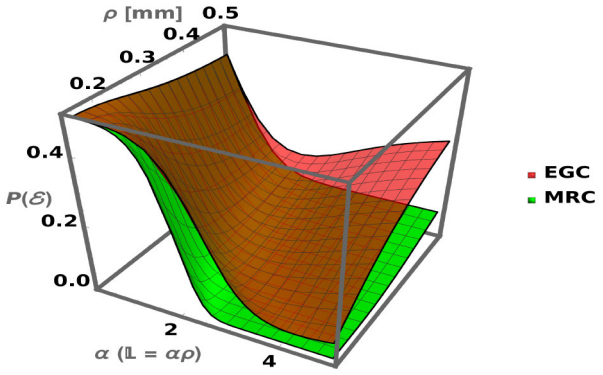

FIGURE 11. This figure plots the error probability as a function of the factor α and beam radius ρ for MRC and EGC schemes.

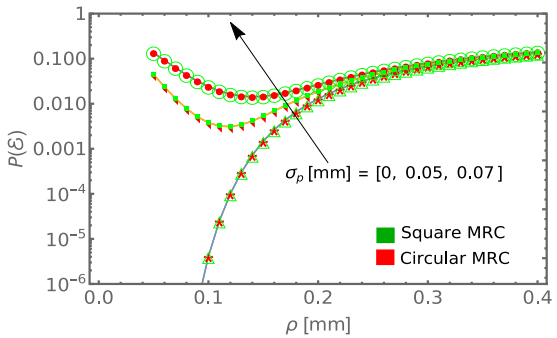

FIGURE 12. This figure shows the probability of error performance of circular and square arrays with the continuous configuration for MRC when the channel suffers from pointing error.

For the continuous array configuration, Fig. 12 represents a comparison of the probability of error performance for the MRC as a function of beam or spot radius ρ for different values of the pointing error standard deviation σ_p. In the same figure, we also consider a performance comparison of rectangular and circular arrays when the areas of both the arrays are equal. Additionally, in Fig. 13. we compare the error rate performance of the EGC and MRC schemes for the continuous array configuration when the channel suffers from pointing errors. For both the figures, the area of the arrays is $\mathcal{A} = 4$ mm^2, the noise power $\sigma_n = 0.1$ W/mm^2, and the total signal power is 1 W.

We note from Fig. 12 that there is an optimal value of ρ—which we denote by ρ^*—that will minimize the error probability, and this optimal value depends on the value of the pointing error standard deviation σ_p: a larger value of σ_p indicates that we should choose a larger spot radius ρ^* in order to minimize the effect of the pointing error. We note that the error probability performance of circular and square arrays is almost similar for all values of pointing error standard deviation considered in the experiment.

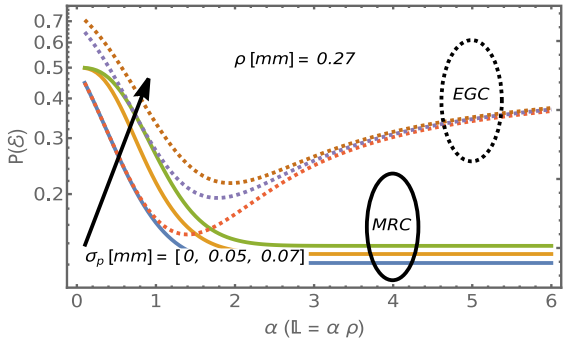

FIGURE 13. This figure compares the error probability performance of EGC and MRC schemes for continuous arrays as a function of the parameter α when pointing error is present in the channel.

V. COMPLEXITY ANALYSIS

This section briefly analyzes the complexity of different combining schemes for an array of detectors. Since the EGC combines the outputs of all the array elements to form a sufficient statistic, it can do so without storing each of the element outputs. All the outputs can be combined at the circuit level without using any computational resources. Thus, the computational complexity of EGC is $O(1)$, where O denotes Big O notation. Regarding the SC, both the Max SNR and Max Output versions require a sorting algorithm to find the maximum of the M output values. Therefore, the selection combiner has a complexity of $O(M \log(M))$ if we use merge sorting. For the MRC, we have M multiplications and M additions, and therefore, its complexity is $O(M)$.

The SC (Max SNR) and MRC incur additional complexity since they require the estimation of beam parameters—such as peak intensity λ_p, the beam radius ρ and the location of the beam center (x_0, y_0) on the array—in order to form the sufficient statistic. The value of beam radius ρ in the focal plane depends on the focal length of the lens; hence it is treated as a known deterministic quantity. The estimation of λ_p is straightforward via a method of moments estimator [2], and we may ignore its complexity. Regarding the estimation of (x_0, y_0), if we use a centroid estimator, we need a total of $3M$ additions and $2M$ multiplications (please see the definition of the centroid estimator in [3] or [4]). However, if a beam center is estimated using a maximum likelihood estimator, the complexity is $O(|\mathcal{A}|^2 M) + O(|\mathcal{A}|^3)$ [2]. Thus, this extra complexity has to be incorporated into the total complexity of MRC and SC (Max SNR) schemes.

Additionally, we want to point out that there is a hardware complexity associated with an array of detectors. For instance, if the number of detectors is enormous, the optical fill factor might be too small. Thus, we may place a microlens array in front of the array of detectors to focus the energy away from the dead area into the active area (the detectors). This will minimize the effect of a reduced optical fill factor.

Scheme	Complexity
EGC	$O(1)$
MRC	$O(M) + O(\|\mathcal{A}\|^2 M) + O(\|\mathcal{A}\|^3)$
SC (Max Output)	$O(M \log(M))$
SC (Max SNR)	$O(M \log(M)) + O(\|\mathcal{A}\|^2 M) + O(\|\mathcal{A}\|^3)$

FIGURE 14. This table summarizes the computational complexity of different combining schemes.

Fig. 14 summarizes the complexities of different combining schemes for an array of detectors and a single detector.

VI. CONCLUSION AND FUTURE WORK

In this paper, we have analyzed the performance of a detector array receiver in a free-space optical communication system for different data combining schemes. The different combining schemes considered were the equal gain combining (EGC), selection combining (SC) (max SNR), selection combining (Max Output), and the maximal ratio combiner (MRC). We observe that all schemes provide good performance when the SNR is high; however, the difference in performance becomes significant at low SNR. We note that when the SNR is low, the MRC performed better than all other combining schemes in terms of error rate performance, and the EGC yielded the least performance gain. However, under the special case when the element or detector size was much smaller than the spot size, both versions of the selection combining schemes broke down in error probability performance. However, the performance of MRC only improves with a smaller detector size whereas the performance of the EGC is independent of the spot size to detector size ratio. Finally, when EGC is applied to the limiting or continuous array scenario, a certain array area will minimize the error probability. This optimum area is proportional to the square of the beam radius. For a channel that suffers from pointing errors, the optimal spot radius is directly proportional to the pointing error standard deviation.

In terms of computational complexity, EGC uses up the least computational resources ($O(1)$) followed by the MRC scheme (O(M)), which is followed by the SC schemes ($O(M \log(M))$).

In light of the above, we propose a hybrid switching scheme based on EGC and MRC for an array of detectors receiver where the switch shifts between EGC and MRC schemes depending on the available SNR. The switch connects to EGC for high SNR and resorts to the MRC when the SNR goes below a certain threshold.

In the future, we will analyze the performance of these combining schemes and optimize beam parameters in the presence of pointing errors and channel fading in terrestrial free-space optical communications.

REFERENCES

[1] A. Trichili, M. A. Cox, B. S. Ooi, and M.-S. Alouini, "Roadmap to free space optics," *J. Opt. Soc. Amer. B*, vol. 37, no. 11, pp. A184–A201, Nov. 2020. [Online]. Available: http://josab.osa.org/abstract.cfm?URI=josab-37-11-A184

[2] M. S. Bashir, M.-C. Tsai, and M.-S. Alouini, "Cramér–Rao bounds for beam tracking with photon counting detector arrays in free-space optical communications," *IEEE Open J. Commun. Soc.*, vol. 2, pp. 1065–1081, 2021.

[3] D. L. Snyder and M. I. Miller, *Random Point Processes in Time and Space*. New York, NY, USA: Springer-Verlag, 1991.

[4] M. S. Bashir and M. R. Bell, "Optical beam position estimation in free-space optical communication," *IEEE Trans. Aerosp. Electron. Syst.*, vol. 52, no. 6, pp. 2896–2905, Dec. 2016.

[5] M. S. Bashir and M. R. Bell, "Optical beam position tracking in free-space optical communication systems," *IEEE Trans. Aerosp. Electron. Syst.*, vol. 20, no. 2, pp. 520–536, Apr. 2018.

[6] M. S. Bashir and M. R. Bell, "The impact of optical beam position estimation on the probability of error in free-space optical communications," *IEEE Trans. Aerosp. Electron. Syst.*, vol. 55, no. 3, pp. 1319–1333, Jun. 2019.

[7] M. S. Bashir and S. S. Muhammad, "Time synchronization in photon-limited deep space optical communications," *IEEE Trans. Aerosp. Electron. Syst.*, vol. 56, no. 1, pp. 30–40, Feb. 2020.

[8] M. S. Bashir, "Free-space optical communications with detector arrays: A mathematical analysis," *IEEE Trans. Aerosp. Electron. Syst.*, vol. 56, no. 2, pp. 1420–1429, Apr. 2020.

[9] M. S. Bashir and M.-S. Alouini, "Signal acquisition with photon-counting detector arrays in free-space optical communications," *IEEE Trans. Wireless Commun.*, vol. 19, no. 4, pp. 2181–2195, Apr. 2020.

[10] M. S. Bashir and M. S. Alouini, "Free-space optical MISO communications with an array of detectors," *IEEE Open J. Commun. Soc.*, vol. 1, pp. 1765–1780, 2020.

[11] V. A. Vilnrotter and M. Srinivasan, "Adaptive detector arrays for optical communications receivers," *IEEE Trans. Commun.*, vol. 50, no. 7, pp. 1091–1097, Jul. 2002.

[12] V. Vilnrotter, C.-W. Lau, M. Srinivasan, K. Andrews, and R. Mukai, "Optical array receiver for communication through atmospheric turbulence," *J. Lightw. Technol.*, vol. 23, no. 4, pp. 1664–1675, Apr. 2005.

[13] M. Srinivasan, K. S. Andrews, W. H. Farr, and A. Wong, "Photon counting detector array algorithms for deep space optical communications," in *Proc. SPIE*, vol. 9739, 2016, pp. 267–282. [Online]. Available: https://doi.org/10.1117/12.2217971

[14] K. Kiasaleh, "Nonlinear array detection strategies for optical beams in long range fee-space optics channels," in *Proc. Int. Conf. Space Opt. (ICSO)*, vol. 11180, 2019, pp. 2068–2078. [Online]. Available: https://doi.org/10.1117/12.2536124

[15] K. Kiasaleh, "Agile optical receiver with detector arrays optimized using particle swarm optimization," in *Proc. Int. Conf. Space Opt. (ICSO)*, vol. 11180, 2019, pp. 1–12.

[16] K. Kiasaleh, "A novel detection strategy for optical receivers with focal plane array," in *Proc. Int. Conf. Space Opt. (ICSO)*, vol. 11852, 2021, pp. 2271–2281. [Online]. Available: https://doi.org/10.1117/12.2599960

[17] A. A. Farid and S. Hranilovic, "Outage capacity optimization for free-space optical links with pointing errors," *J. Lightw. Technol.*, vol. 25, no. 7, pp. 1702–1710, Jul. 2007.

[18] V. V. Mai and H. Kim, "Adaptive beam control techniques for airborne free-space optical communication systems," *Appl. Opt.*, vol. 57, no. 26, pp. 7462–7471, Sep. 2018.

[19] M.-S. Alouini and M. K. Simon, "Performance of generalized selection combining over Weibull fading channels," in *Proc. IEEE 54th Veh. Technol. Conf. VTC Fall*, vol. 3, 2001, pp. 1735–1739.

[20] M. K. Simon and M.-S. Alouini, "Performance analysis of generalized selection combining with threshold test per branch (T-GSC)," in *Proc. IEEE Global Telecommun. Conf. (GLOBECOM)*, vol. 2, 2001, pp. 1176–1181.

[21] H.-C. Yang and M.-S. Alouini, "MRC and GSC diversity combining with an output threshold," *IEEE Trans. Veh. Technol.*, vol. 54, no. 3, pp. 1081–1090, May 2005.

[22] J. Goodman, *Statistical Optics* (Wiley Series in Pure and Applied Optics). Hoboken, NJ, USA: Wiley, 2015. [Online]. Available: https://books.google.com.sa/books?id=9Ol8CAAAQBAJ

[23] M. S. Bashir and M.-S. Alouini, "Optimal power allocation between beam tracking and symbol detection channels in a free-space optical communications receiver," *IEEE Trans. Commun.*, vol. 69, no. 11, pp. 7631–7646, Nov. 2021.

MING-CHENG TSAI (Graduate Student Member, IEEE) was born in Fujian, China. He received the B.E. degree in electrical engineering from the National Taipei University of Technology, Taipei, Taiwan, in 2015, and the master's degree from the King Abdullah University of Science and Technology in 2020, where he is currently pursuing the Ph.D. degree in electrical engineering. From 2015 to 2018, he was a student of Communication Engineering with National Tsinghua University. His current research interests include free-space optical, signal processing for tracking systems, and estimation theory.

MUHAMMAD SALMAN BASHIR (Senior Member, IEEE) received the M.S. and Ph.D. degrees in electrical and computer engineering from Purdue University, West Lafayette, IN, USA, in 2014 and 2017, respectively. He served as a Faculty Member with the National University of Computer and Emerging Sciences Lahore, before joining the Communication Theory Lab, King Abdullah University of Science and Technology, Thuwal, Saudi Arabia, as a Postdoctoral Fellow in 2019. His current research interests are in the area of statistical signal processing, optimization, and information theory for wireless communications. He was the recipient of the International Fulbright Science and Technology Award for his graduate studies at Purdue University.

MOHAMED-SLIM ALOUINI (Fellow, IEEE) was born in Tunis, Tunisia. He received the Ph.D. degree in electrical engineering from the California Institute of Technology in 1998. He served as a Faculty Member with the University of Minnesota then with Texas A&M University at Qatar before joining the King Abdullah University of Science and Technology in 2009, where he is currently a Distinguished Professor of Electrical and Computer Engineering. He is currently particularly interested in addressing the technical challenges associated with the uneven distribution, access to, and use of information and communication technologies in far-flung, rural, low-density populations, low-income, and/or hard-to-reach areas. He is a Fellow of OSA.